ACS Photonics

Letter

Cite This: ACS Photonics XXXX, XXX, XXX−XXX

Hybrid Plasmonic Bullseye Antennas for Efficient Photon Collection

Sebastian K. H. Andersen,[*,†] Simeon Bogdanov,[‡] Oksana Makarova,[‡] Yi Xuan,[‡] Mikhail Y. Shalaginov,[‡] Alexandra Boltasseva,[‡] Sergey I. Bozhevolnyi,[†] and Vladimir M. Shalaev[‡]

[†]Center for Nano Optics, University of Southern Denmark, DK-5230 Odense M, Denmark

[‡]School of Electrical and Computer Engineering, Purdue Quantum Center, Purdue University, West Lafayette, Indiana 47907, United States

Supporting Information

ABSTRACT: We propose highly efficient hybrid plasmonic bullseye antennas for collecting photon emission from nm-sized quantum emitters. In our approach, the emitter radiation is coupled to surface plasmon polaritons that are consequently converted into highly directional out-of-plane emission. The proposed configuration consists of a high-index titania bullseye grating separated from a planar silver film by a thin low-index silica spacer layer. Such hybrid systems are theoretically capable of directing 85% of the dipole emission into a 0.9 NA objective, while featuring a spectrally narrow-band tunable decay rate enhancement of close to 20 at the design wavelength. Hybrid antenna structures were fabricated by standard electron-beam lithography without the use of lossy adhesion layers that might be detrimental to antenna performance. The fabricated antennas remained undamaged at saturation laser powers exhibiting stable operation. For experimental characterization of the antenna properties, a fluorescent nanodiamond containing multiple nitrogen vacancy centers (NV-center) was deterministically placed in the bullseye center, using an atomic force microscope. Probing the NV-center fluorescence we demonstrate resonantly enhanced, highly directional emission at the design wavelength of 670 nm, whose characteristics are in excellent agreement with our numerical simulations.

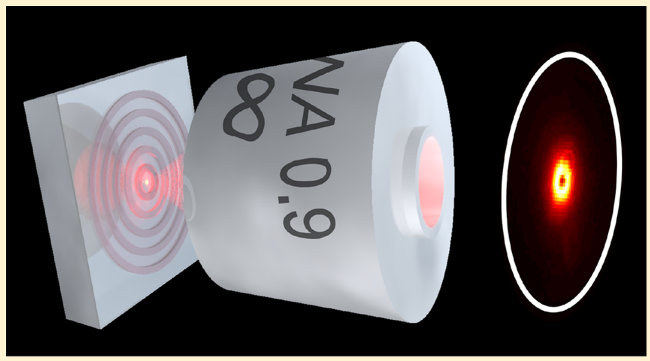

KEYWORDS: *plasmonics, collection efficiency, nitrogen-vacancy center, quantum emitter, fluorescence*

Efficient collection of photons from single quantum emitters (QE) is a key requirement for many quantum technological applications,[1] utilizing on-demand photon generation, optical spin read-out,[2,3] or coalescence of indistinguishable photons.[4,5] The efficiency by which photons can be collected is, however, often compromised by the nonunity quantum yield and relatively omnidirectional emission pattern of typical QEs, whether it is a molecule, quantum dot, or solid state defect.[6] Fortunately, both aspects can be improved upon by engineering the photonic environment. Quantum yield may be increased by accelerating the radiative spontaneous decay rate, relative to intrinsic nonradiative decay, via the Purcell effect.[7] Directional emission is typically achieved by two approaches:[8] either a geometrical- or a mode-coupling approach. The geometrical approach relies on redirecting far-field emission by reflection or refraction on appropriately shaped surfaces, such as a parabolic mirror[9] or solid immersion lens.[10] Alternatively, the mode-coupling approach is based on near-field coupling QE emission to an antenna or waveguide mode. The emission pattern then conforms to that of the antenna,[11] while for detection with an objective, plane film waveguide modes may be redirected to free space by leakage into high index substrates[12] or scattering on periodic gratings.[13,14] For highly directional emission, the circular symmetric bullseye grating is particularly attractive as tight beaming of photons is achievable by appropriate grating design. Bullseye gratings have been utilized for photon collection from QEs in dielectric membranes[13,14] or situated near a grating imprinted in a metal film. Here we consider the metallic counterpart. Metallic bullseye designs currently fall in two categories. The first category consists of an aperture in a metal film, encircled by a bullseye grating.[15−17] This so-called bullseye aperture configuration features both large decay rate enhancement and highly directional emission from QEs situated in the aperture, however the antenna efficiency suffers from large ohmic losses. Single photon emission from such a configuration was demonstrated by Choy et al., considering a nitrogen-vacancy center (NV-center) in a diamond/silver-aperture.[17] The design theoretically allowed for a decay rate enhancement of ∼25 (relative to bulk diamond) and collection of ∼17% of dipole emission with a 0.6 NA objective. Photon collection being compromised by reflections from the diamond/air interface appearing before the objective, and high losses of plasmon modes supported by diamond/silver interface. More recently, a second design, consisting of a quantum dot situated in a dielectric film above a silver film

Received: October 11, 2017
Published: January 7, 2018

DOI: 10.1021/acsphotonics.7b01194
ACS Photonics XXXX, XXX, XXX−XXX

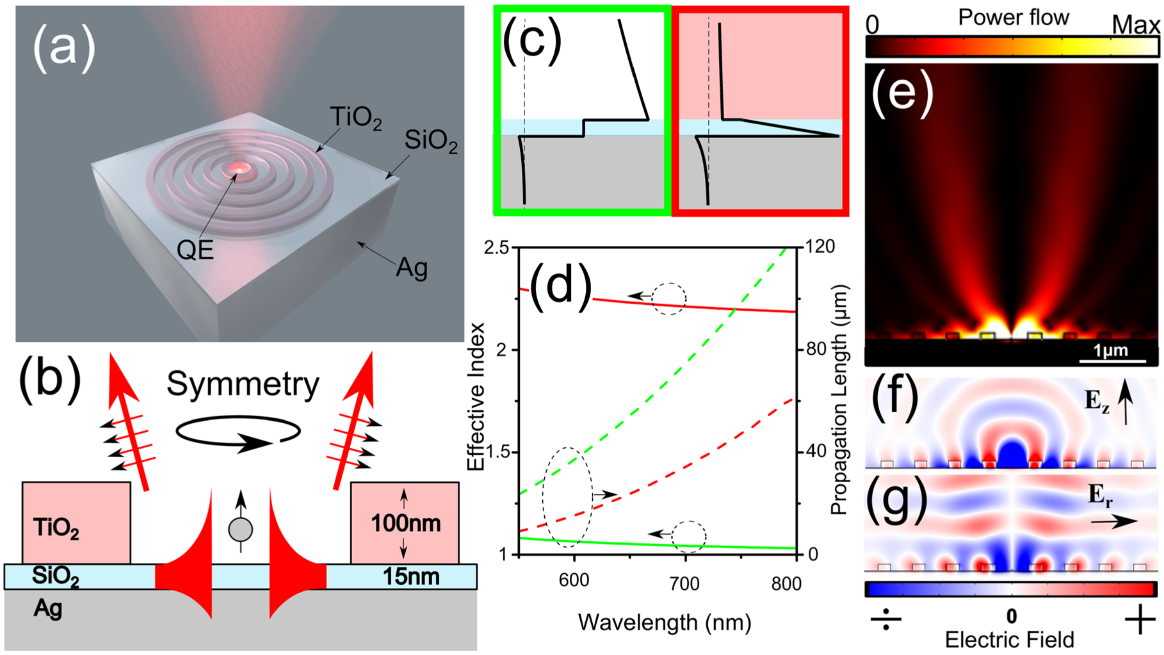

Figure 1. (a) Concept image of bullseye structure. Spontaneous emission from a centered quantum emitter is efficiently directed into the collection optics, as SPP-coupled emission scatters on the periodic ridges. (b) Profile view of the rotationally symmetric structure, emission is numerically modeled for a vertical dipole aligned with the symmetry axis. (c) Analytical out-of-plane electric field distribution for SPP modes supported by semi-infinite air (green) or TiO_2 (red) top layer on a 15 nm SiO_2 spacer, and semi-infinite bottom Ag layer. (d) Corresponding effective index (solid) and propagation length (dashed). (e) On resonance power density flow of optimized antenna with corresponding (f) out-of-plane and (g) radial electric field distributions.

bullseye grating, has been explored by Livneh et al., as a way to circumvent metal losses.[18,19] Exceptionally directional beaming of single photons has been demonstrated by this design, allowing for ~37% of dipole emission to be collected with a 0.65 NA objective, while no decay rate enhancement was reported. The combination of appreciable decay rate enhancement and low-loss directive photon generation thus appears elusive from previous metal bullseye designs, while both are desirable to boost quantum yield and collection efficiency, respectively. Further, a common characteristic of these previous bullseye designs is the corrugation of the metal film. However, recently such structuring of silver films has been observed to be problematic for single photon applications, as corrugating silver films, either by focused ion beam milling or standard electron beam lithography, result in a significant background, detrimental for single photon applications.[18,20] Antenna designs compatible with fabrication techniques which yield low background emission levels are therefore highly desirable for quantum photonics. Though novel fabrication techniques may improve background levels from corrugated silver,[21] antenna designs based on planar silver films is an appealing approach, as background is significantly reduced compared to a corrugated surface.[18] Further planar film designs are readily compatible with high-quality monocrystalline silver film fabrication techniques.[22] While a variety of plasmonic antenna designs based on patterned metal films and/or metal nanoparticles has been realized, the planar silver film antenna employing a dielectric bullseye grating has not been explored.

In this study, we propose a hybrid plasmonic bullseye antenna design based on a planar silver film, employing a high-index, 100 nm-thick, dielectric, titania (TiO_2) bullseye grating, situated on a low-index, 15 nm-thin spacer layer, made of silica (SiO_2). The configuration combines low antenna loss and highly directional emission with a moderate decay rate enhancement. Theoretically, 85% of the QE emission may be collected by a 0.9 NA objective lens, while the photon emission rate is accelerated by a decay rate enhancement of 18 (relative to vacuum), at the design wavelength of 670 nm. The design inherently ensures environmental protection of silver, by consequence of the protective silica layer, while the particular choice of materials allows for fabrication without compromising antenna performance by the use of lossy adhesion layers and stable operation at a laser power of 2.5 mW corresponding to saturation of NV-center fluorescence. For experimental demonstration of the design, a nanodiamond (ND) containing a large number of NV-centers was deterministically placed in the center of the bullseye, using an atomic force microscope. Spectrally resolving NV-center emission, a resonant enhancement peak (quality factor ~ 18) is observed at the design wavelength. The on-resonance emission is selected with a band-pass filter and confirmed to be highly directional by back-focal plane imaging, with the overall emission pattern closely following numerical predictions. Specifically, emission takes the form of a radially polarized, donut-shaped beam, imposed by the rotational symmetry of the antenna, with peak emission radiated at an angle of 5° ± 3° fwhm with respect to the plane normal.

RESULTS AND DISCUSSION

The general operation of our device is conceptually illustrated in Figure 1a,b. A QE, centered in the bullseye antenna in close proximity to the silver film, spontaneously decays by excitation of surface plasmon polaritons (SPP) propagating along the dielectric−metal interface. The SPP subsequently scatter directionally on the periodically spaced TiO_2 ridges, resulting in highly directional emission.

DOI: 10.1021/acsphotonics.7b01194
ACS Photonics XXXX, XXX, XXX−XXX

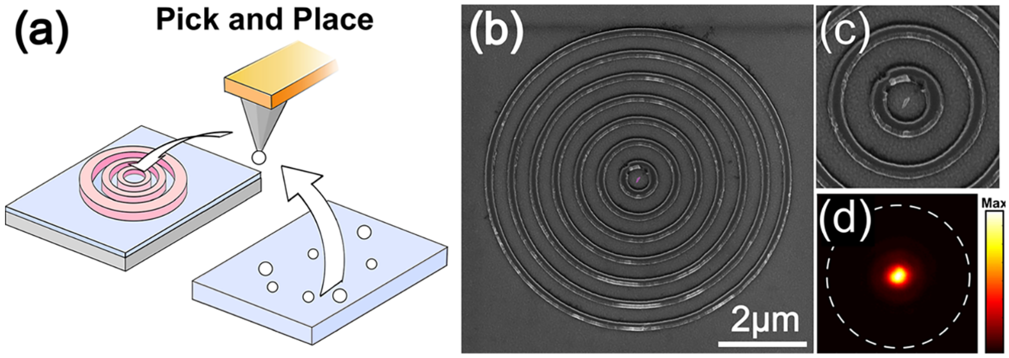

Figure 2. (a) Sketch of AFM "pick and place" technique used in transferring a ND from a coverslip to the bullseye center. (b) Electron micrograph of fabricated bullseye antenna, the transferred ND appears in false color in the center, (c) clearly apparent in the zoomed image. (d) False color CCD image of emission from the ND, dashed line indicates bullseye boundary.

The emission of a QE or electric dipole, situated in close proximity to a silver film, has been thoroughly studied[23] and analytically described.[24,25] It is thus well-known the decay rate is accelerated when the dipole is oriented normal to the metal plane, as beyond photon radiation the dipole may release its energy by SPP emission or nonradiative metal quenching. SPP emission being the dominating decay channel for dipole-metal separations slightly larger than ∼10 nm, ensured here by placing the emitter on top of a thin SiO_2 layer. On the other hand, when the dipole is oriented along the plane, emission is suppressed, as the dipole induces a mirrored antiphase charge distribution in the silver film (see Support Information (SI)). In the present study we thus neglect the weak in-plane dipole emission, and model QE emission solely in terms of the dominating vertical dipole (Figure 1b). Placing the dipole along the symmetry z-axis, our system reduces to a cylindrical symmetric system, for which we assume a constant azimuthal phase, as no particular phase preference can be expected. In other words, the emission field is assumed to be unchanged upon rotation about the z-axis. Clearly, in this case the radial electric field component is singular on the symmetry axis, and must therefore be zero (Figure 1g). The condition prohibits emission along the symmetry axis, as the transverse field of a plane wave, propagating along the symmetry axis, must be zero. The rotational symmetry of dipole source and antenna is thus expected to result in a radially polarized emission field, for which emission normal to the silver film is prohibited, regardless of emission wavelength.

With the symmetry constraints in place, we now seek to maximize dipole emission into the 0.9 NA objective, at the target wavelength of λ_0 = 670 nm, by introducing a dielectric grating for scattering of SPP coupled emission. In order to maximize antenna efficiency, we seek to minimize SPP propagation loss by employing a high-index TiO_2 grating (n = 2.2 index, measured with ellipsometry see SI), separated from the silver film by a thin low-index SiO_2 spacer layer (n = 1.45 index). The SPP mode of the high index-low index spacer - on conductor configuration[26] is receiving increasing interest as a possible approach for low-loss plasmonics.[27,28] Analytical solutions for the SPP mode supported by the 3-layer structure (Figure 1c,d) reveal large modulation of the effective index from $N_{\mathrm{eff}}^{\mathrm{air}}$ = 1.05 (air−SiO_2−Ag) to $N_{\mathrm{eff}}^{\mathrm{TiO_2}}$ = 2.25 (TiO_2−SiO_2−Ag), with propagation lengths of, respectively, $L_{\mathrm{p}}^{\mathrm{air}}$ = 63 μm and $L_{\mathrm{p}}^{\mathrm{TiO_2}}$= 28 μm, far exceeding lateral antenna dimensions. SPP coupled emission is thus prone to either scatter on the TiO_2 grating or reflect back to the emitter, while propagation losses are minimal. For fabrication purposes, we set titania and silica film thicknesses to 100 and 15 nm, respectively, and numerically optimize in-plane grating parameters for collecting the maximal amount of power from a dipole, positioned 15 nm above the SiO_2 film, using a 0.9 NA objective (see SI for optimization procedure). While the vertical dipole position is set to a typical height, expected experimentally, the optimized antenna performance is weakly dependent on the actual position (see SI). For the optimized antenna, the inner TiO_2 ridge (inner radius 250 nm, TiO_2 width 212 nm) forms a standing wave cavity (Figure 1f), accelerating dipole emission by a decay rate enhancement of 18 (relative to vacuum). Simultaneously, the periodic TiO_2 grating (period 520 nm, duty cycle 0.36), directionally scatters SPP coupled emission, such that 85% of the power emitted by the dipole is collected by the objective. While on-resonance SPP emission is scattered at an angle near normal to silver plane (Figure 1e,g), the scattering angle generally seems to follow the grating equation (see SI for comparison). The geometrical optimization of TiO_2 height is a trade-off between decay rate enhancement and collection efficiency. Collection efficiency defined as the fraction of the total dipole power, collected by the objective, while decay rate enhancement is the factor by which the total dipole emission power increases in the bullseye environment, relative to vacuum. Indeed, a significant increase in decay rate enhancement is possible by increasing the TiO_2 thickness (see SI for modeling) at the cost of collection efficiency, as the SPP perform an increasing number of lossy round trips in the cavity before scattering to free space. For practical fabrication purposes, the low aspect ratio design of 100 nm TiO_2 was preferred, while the 15 nm SiO_2 film thickness was set to ensure a homogeneous coverage of the silver film, for environmental protection of the silver.

The bullseye antenna sample was fabricated on a Si substrate by e-beam evaporation of 10 nm Ti, 3 nm Ge, followed by a 200 nm Ag film, and topped by a 15 nm SiO_2 layer, without breaking the vacuum. The Ge layer act as a wetting layer, reducing roughness of the consecutively deposited Ag film.[29] The 100 nm TiO_2 bullseye grating was subsequently formed by standard electron beam lithography and e-beam evaporation (Figure 2b). Importantly, device performance was not degraded by the use of any lossy adhesion layers at the Ag−SiO_2−TiO_2 interfaces, while remaining mechanically robust to sonication, applied during lift-off. A ND (length ∼ 140 nm, height ∼ 35 nm) containing a large number of NV-centers was subsequently picked up from a coverslip and placed in the center of the

DOI: 10.1021/acsphotonics.7b01194
ACS Photonics XXXX, XXX, XXX−XXX

bullseye antenna, using an atomic force microscope (AFM; Figure 2a). The AFM "pick and place" technique[30] allows for precise centering of the ND, as confirmed by electron microscopy (Figure 2d). Pumping the ND with a 532 nm continuous-wave laser, we image the NV-center fluorescence onto a CCD camera, using a 0.9 NA ×100 objective and fluorescence filtering from a dichroic mirror (cutoff 550 nm) and long pass filter (cutoff 550 nm; see SI for thorough method description). NV-center emission is observed as a spot, tightly confined to the center of the antenna (Figure 2c). While fluorescence is weakly observed throughout the whole antenna (see SI for log-scale image), the fast drop-off in fluorescence intensity indicate efficient scattering of SPP emission on the TiO_2 ridges. Correspondingly, antennas without a ND appear dark, when mapping fluorescence by laser-scanning confocal microscopy (see SI for comparison). In order to observe the wavelength dependent decay rate enhancement, expected from numerical modeling (Figure 3a), the NV-center emission was

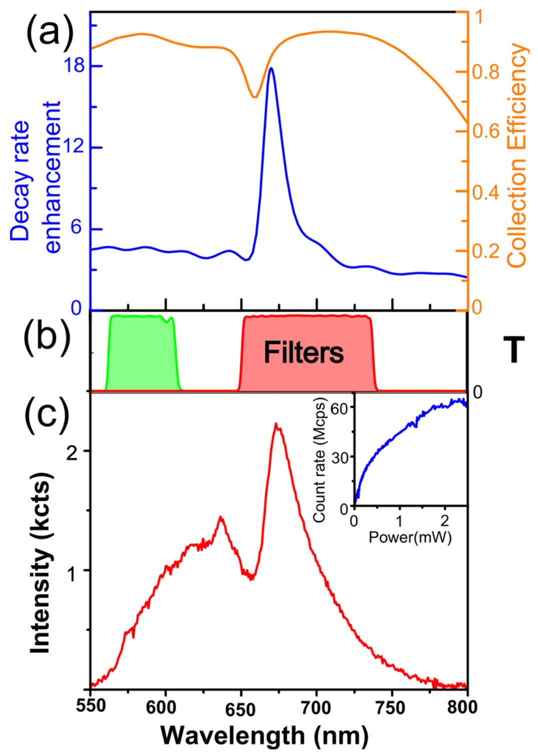

Figure 3. (a) Modeled decay rate enhancement (blue) and collection efficiency (orange) for fabricated bullseye design. (b) Transimission of bandpass filters used for detecting off-resonance (560−610 nm; green) and on-resonance (650−740 nm; red) emission, respectively. (c) Emission spectrum from ND centered in bullseye. Inset shows the background corrected saturation curve, demonstrating stable antenna operation up to saturation laser power.

spectrally resolved on a grating spectrometer (Figure 3c). The zero phonon lines (ZPL) for the neutral (575 nm) and negative (637 nm) charge states confirm the NV-center as the origin of fluorescence, while the overall spectrum is dominated by a resonant enhancement peak at 675 nm, in reasonable agreement with the spectral position and shape of the modeled decay rate enhancement. The experimental quality factor of ∼18 (estimated from spectrum) is broader than the modeled resonance ∼41 (estimated from decay rate enhancement curve), presumably due to fabrication imperfections. Collection efficiency is not expected to significantly affect the spectrum, as modeling finds overall high broadband collections efficiency (Figure 3a), stemming from emission into SPP and grating scattering of SPP into objective both being broadband effects.

For efficient photon generation, it is typically desired to maximize photon rate from the QE, by pumping the QE to saturation. We confirmed that our device is stable under such conditions by increasing laser power to the 2.5 mW limit of our equipment. Simultaneously monitoring the photon rate detected by a avalanche photo diode, we smoothly transition to stable operation at saturation (Figure 3c, inset). Subsequently, reducing laser power, we retrace the saturation curve, thereby confirming no antenna alterations. The planar film bullseye antenna is generally expected to exhibit a higher laser damage threshold, than structured film configurations, as nanostructuring of metals suffer from melting point depression.[31] Having confirmed stable operation at saturation laser power and the presence of resonantly enhanced emission, we proceed by examining the off- and on-resonance emission pattern, selected with bandpass filter in the wavelength range 560−610 nm and 650−740 nm (Figure 3b). Introducing a bertrand lens in infinity space, we resolve the emission pattern by imaging the back-focal plane (BFP) of the objective onto the CCD camera (Figure 4a). This lens configuration is particularly well suited for Fourier microscopy.[32] Filtering for resonant emission reveals a highly directional radiation pattern in the characteristic donut-shaped pattern, imposed by the antenna symmetry (Figure 4d). Introducing an analyzer in the optical path, the radiation is confirmed to be radially polarized (Figure 4e,f). This is apparent as emission is spatially extinguished along the axis normal to the analyzer axis for a random analyzer orientation. For a comparison with the numerical design, we extracted the angular radiation pattern from a single pixel slice of the BFP-image, finding the experiment generally replicates numerical expectations. On resonance, the peak emission is detected at an angle of 5° ± 3° fwhm wrt. the plane normal, in good agreement with the designed emission angle of 6° ± 4° fwhm, modeled for the resonance wavelength of 670 nm (Figure 4g). Probing off-resonant emission, we find the peak emission increasing to an angle of 14° ± 8° fwhm (Figure 4k), while the symmetry conditioned, radially polarized donut shaped beam pattern is conserved (Figure 4h−j). Off-resonance emission is in line with the modeled emission for a wavelength of 610 nm having peak emission at an angle of 16° ± 5°. Off-resonance emission is modeled at the wavelength of 610 nm, as experimentally, the maximum spectral power transmitted by the band-pass filter is found at this wavelength (Figure 3c). The directional emission is in stark contrast to the nondirectional emission observed from the same type of ND in the absence of a bullseye antenna (Figure 4b,c). The agreement of the experimental case considering an ensemble of relatively randomly oriented dipole emitters and the numerical model of a vertical dipole, result from the selective radiative enhancement/suppression of emitters with a predominately vertical/horizontal dipole moment, given efficient coupling to SPP or destructive interference. The fluorescence signal dominated by vertical dipoles, thereby mimic the numerical model considering only a vertical dipole. Indeed the particularly broad decay rate distribution, observed for the ND placed in the antenna, does indicate an enhancement/suppression of decay rates (see SI). The antenna performance on a single emitter level is therefore expected to strongly depend on the dipole orientation.

DOI: 10.1021/acsphotonics.7b01194
ACS Photonics XXXX, XXX, XXX−XXX

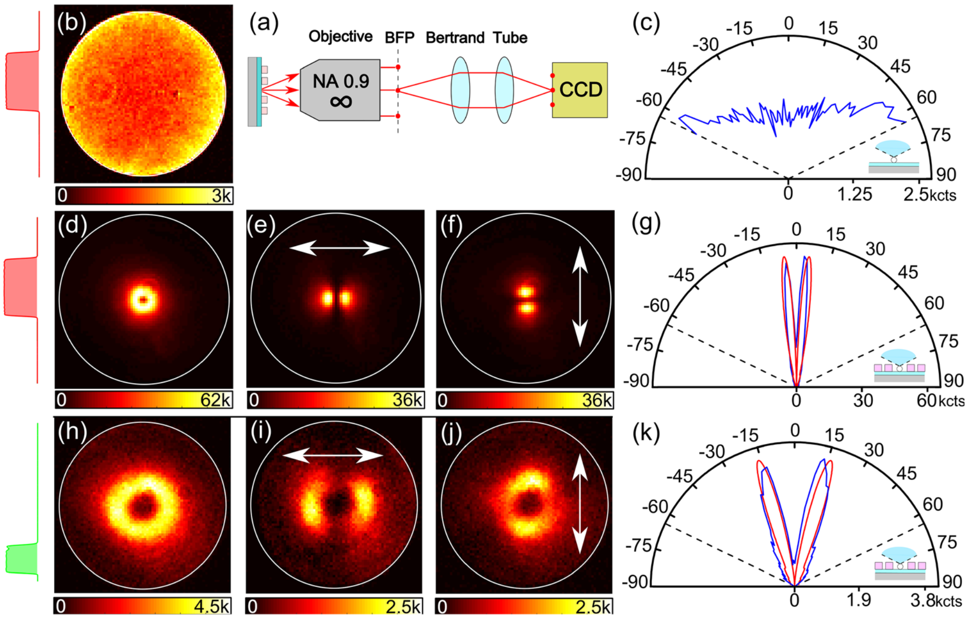

Figure 4. (a) Schematic of experimental setup for back-focal plane (BFP) imaging. (b) Reference BFP-image from ND, without antenna, on the plane SiO_2/Ag sample and (c) corresponding emission pattern, filtered for on-resonance emission. The detection limit of the 0.9 numerical aperture of the objective is indicated by respectively a white circle or black dashed lines. BFP-images filtered for (d−f) on- and (h−j) off-resonance emission from ND in bullseye, imaged with (e, i) horizontal or (f, j) vertical analyzer. Experimental (blue) and modeled (red) emission patterns for (g) on-resonance, model wavelength 670 nm and (k) off-resonance regime, model wavelength 610 nm. BFP images are obtained at 28 μW laser power and 10 s integration time, while colorbars give the camera counts.

The relatively narrowband decay rate enhancement and directive emission, demonstrated for this design, may be of interest for indistinguishable photon experiments, as the selective enhancement and efficient collection of ZPL photons from solid state emitters is desirable. The simple fabrication allows for easy tuning of the antenna resonance to the ZPL of new promising QEs such as the silicon- or germanium vacancy centers.[33,34] However, for scalable single photon source fabrication, large-scale QE positioning techniques need to be explored. Potential approaches may be lithographic patterning[35] or electro-static pad positioning.[36] Further, the highly directional emission pattern should lend itself to optical fiber coupling. Theoretically, 23% and 74% of dipole emission (wavelength 670 nm) fall within the numerical aperture of respectively a single- (NA 0.12) or multimode fiber (NA 0.4). It is in this context worth noting that the radially polarized emission pattern, inherent to the bullseye antenna, may be converted to the fundamental mode of an optical fiber with high fidelity.[37] Directive emission is further advantageous for NV ensemble-based sensing applications, relying on optical read-out of the NV-center spin state, where strong decay rate enhancement should be avoided.[3]

CONCLUSION

In summary, we have proposed a high-efficiency hybrid plasmonic bullseye antenna design, consisting of a high-index titania grating, separated from a planar silver film by a thin low-index silica spacer layer. The architecture is motivated by previous issues with background emission resulting from nanostructuring of silver films. Our design combines low antenna loss, directional emission and moderate decay rate enhancement, leading to a theoretical collection efficiency of 85% for a 0.9 NA objective and acceleration of the emission rate by a decay rate enhancement of 18, at the design wavelength of 670 nm. The design is experimentally realized by standard electron beam lithography, followed by deterministic placement of a fluorescent ND in the bullseye, using the AFM "pick and place" technique. The particular material design allows for fabrication without lossy adhesion layers compromising device performance, and stable operation of the antenna at laser powers large enough for saturated pumping of the NV-centers contained in the ND. Decay rate enhancement is experimentally observed as a resonant peak in the NV-center emission spectrum at 675 nm (quality factor ∼ 18). The resonantly filtered fluorescence is demonstrated to be highly directional by back-focal plane imaging, with peak emission at an angle of 5° with respect to plane normal. Specifically, the emission pattern takes the form of a donut-shaped, radially polarized beam as imposed by the antenna symmetry, regardless of emission wavelength. Experimental observations closely mimic the numerical design, thereby validating the proposed design. However, further experiments must be conducted using single emitters in order to experimentally quantify collection efficiency of the antenna. The demonstrated design is significant for quantum technological development, as light-matter interfaces ensuring efficient photon collection from single QEs are highly desirable for quantum optical applications.

ASSOCIATED CONTENT

Supporting Information

The Supporting Information is available free of charge on the ACS Publications website at DOI: 10.1021/acsphotonics.7b01194.

S1: Schematic of experimental setup. S2: Analytical model of electric dipole above silver film. S3: Ellipsometry measurement of TiO_2 refractive index. S4: Numerical optimization procedure of bullseye antenna. S5: Antenna performance as function vertical dipole position S6: Comparison of bullseye emission angle with grating equation. S7: Optimized antenna design for different TiO_2 heights. S8: Antenna fluorescence image in log scale S9: Confocal scan of bullseye antenna with- and without ND. S10: Lifetime distribution measurements (PDF).

AUTHOR INFORMATION

Corresponding Author

*E-mail: sekh@mci.sdu.dk.

ORCID

Sebastian K. H. Andersen: 0000-0003-4566-6036

Sergey I. Bozhevolnyi: 0000-0002-0393-4859

Notes

The authors declare no competing financial interest.

ACKNOWLEDGMENTS

The authours gratefully acknowledge the finanical support of the European Research Council (Grant 341054 (PLAQNAP)), Georgia St. (Grant 106806), MRSEC (Grant 105675), ONR-DURIP (Grant No. N00014-16-1-2767), AFOSR-MURI (Grant No. FA9550-14-10389), and DOE (Grant DE-SC0017717).

ABBREVIATIONS

QE	quantum emitter
TiO_2	titania
SiO_2	silica
SI	Supporting Information
NV-center	nitrogen vacancy center
ND	nanodiamond
BFP	back focal plane
AFM	atomic force microscope
ZPL	zero phonon line
SPP	surface plasmon polariton

REFERENCES

(1) O'Brien, J. L.; Furusawa, A.; Vuckovic, J. Photonic quantum technologies. *Nat. Photonics* **2009**, *3*, 687−695.

(2) Steiner, M.; Neumann, P.; Beck, J.; Jelezko, F.; Wrachtrup, J. Universal enhancement of the optical readout fidelity of single electron spins at nitrogen-vacancy centers in diamond. *Phys. Rev. B: Condens. Matter Mater. Phys.* **2010**, *81*, 035205.

(3) Bogdanov, S.; Shalaginov, M. Y.; Akimov, A.; Lagutchev, A. S.; Kapitanova, P.; Liu, J.; Woods, D.; Ferrera, M.; Belov, P.; Irudayaraj, J.; Boltasseva, A.; Shalaev, V. M. Electron spin contrast of Purcell-enhanced nitrogen-vacancy ensembles in nanodiamonds. *Phys. Rev. B: Condens. Matter Mater. Phys.* **2017**, *96*, 035146.

(4) Bernien, H.; Childress, L.; Robledo, L.; Markham, M.; Twitchen, D.; Hanson, R. Two-Photon Quantum Interference from Separate Nitrogen Vacancy Centers in Diamond. *Phys. Rev. Lett.* **2012**, *108*, 043604.

(5) Sipahigil, A.; Jahnke, K. D.; Rogers, L. J.; Teraji, T.; Isoya, J.; Zibrov, A. S.; Jelezko, F.; Lukin, M. D. Indistinguishable Photons from Separated Silicon-Vacancy Centers in Diamond. *Phys. Rev. Lett.* **2014**, *113*, 113602.

(6) Aharonovich, I.; Englund, D.; Toth, M. Solid-state single-photon emitters. *Nat. Photonics* **2016**, *10*, 631−641.

(7) Kinkhabwala, A.; Yu, Z.; Fan, S.; Avlasevich, Y.; Mullen, K.; E, M. Large single-molecule fluorescence enhancements produced by a bowtie nanoantenna. *Nat. Photonics* **2009**, *3*, 654−657.

(8) Barnes, W.; Björk, G.; Gérard, J.; Jonsson, P.; Wasey, J.; Worthing, P.; Zwiller, V. Solid-state single photon sources: light collection strategies. *Eur. Phys. J. D* **2002**, *18*, 197−210.

(9) Schell, A. W.; Neumer, T.; Shi, Q.; Kaschke, J.; Fischer, J.; Wegener, M.; Benson, O. Laser-written parabolic micro-antennas for efficient photon collection. *Appl. Phys. Lett.* **2014**, *105*, 231117.

(10) Jamali, M.; Gerhardt, I.; Rezai, M.; Frenner, K.; Fedder, H.; Wrachtrup, J. Microscopic diamond solid-immersion-lenses fabricated around single defect centers by focused ion beam milling. *Rev. Sci. Instrum.* **2014**, *85*, 123703.

(11) Curto, A. G.; Volpe, G.; Taminiau, T. H.; Kreuzer, M. P.; Quidant, R.; van Hulst, N. F. Unidirectional Emission of a Quantum Dot Coupled to a Nanoantenna. *Science* **2010**, *329*, 930−933.

(12) Lee, K. G.; Chen, X. W.; Eghlidi, H.; Kukura, P.; Lettow, R.; Renn, A.; Sandoghdar, V.; Gotzinger, S. A planar dielectric antenna for directional single-photon emission and near-unity collection efficiency. *Nat. Photonics* **2011**, *5*, 166−169.

(13) Li, L.; Chen, E. H.; Zheng, J.; Mouradian, S. L.; Dolde, F.; Schröder, T.; Karaveli, S.; Markham, M. L.; Twitchen, D. J.; Englund, D. Efficient Photon Collection from a Nitrogen Vacancy Center in a Circular Bullseye Grating. *Nano Lett.* **2015**, *15*, 1493−1497.

(14) Davanço, M.; Rakher, M. T.; Schuh, D.; Badolato, A.; Srinivasan, K. A circular dielectric grating for vertical extraction of single quantum dot emission. *Appl. Phys. Lett.* **2011**, *99*, 041102.

(15) Aouani, H.; Mahboub, O.; Bonod, N.; Devaux, E.; Popov, E.; Rigneault, H.; Ebbesen, T. W.; Wenger, J. Bright Unidirectional Fluorescence Emission of Molecules in a Nanoaperture with Plasmonic Corrugations. *Nano Lett.* **2011**, *11*, 637−644.

(16) Jun, Y. C.; Huang, K. C.; Brongersma, M. L. Plasmonic beaming and active control over fluorescent emission. *Nat. Commun.* **2011**, *2*, 1−6.

(17) Choy, J. T.; Bulu, I.; Hausmann, B. J. M.; Janitz, E.; Huang, I.-C.; Loncar, M. Spontaneous emission and collection efficiency enhancement of single emitters in diamond via plasmonic cavities and gratings. *Appl. Phys. Lett.* **2013**, *103*, 161101.

(18) Livneh, N.; Harats, M. G.; Istrati, D.; Eisenberg, H. S.; Rapaport, R. Highly Directional Room-Temperature Single Photon Device. *Nano Lett.* **2016**, *16*, 2527−2532.

(19) Livneh, N.; Harats, M. G.; Yochelis, S.; Paltiel, Y.; Rapaport, R. Efficient Collection of Light from Colloidal Quantum Dots with a Hybrid Metal Dielectric Nanoantenna. *ACS Photonics* **2015**, *2*, 1669−1674.

(20) Kumar, S.; Lu, Y.-W.; Huck, A.; Andersen, U. L. Propagation of plasmons in designed single crystalline silver nanostructures. *Opt. Express* **2012**, *20*, 24614−24622.

(21) Nagpal, P.; Lindquist, N. C.; Oh, S.-H.; Norris, D. J. Ultrasmooth Patterned Metals for Plasmonics and Metamaterials. *Science* **2009**, *325*, 594−597.

(22) Park, J. H.; Ambwani, P.; Manno, M.; Lindquist, N. C.; Nagpal, P.; Oh, S.-H.; Leighton, C.; Norris, D. J. Single-Crystalline Silver Films for Plasmonics. *Adv. Mater.* **2012**, *24*, 3988−3992.

(23) Drexhage, K. Influence of a dielectric interface on fluorescence decay time. *J. Lumin.* **1970**, *1*, 693−701.

(24) Ford, G.; Weber, W. Electromagnetic interactions of molecules with metal surfaces. *Phys. Rep.* **1984**, *113*, 195−287.

(25) Chance, R. R.; Proc, A.; Silbey, R. Molecular fluorescence and energy transfer near interfaces. *Adv. Chem. Phys.* **1978**, *37*, 1−34.

(26) Avrutsky, I.; Soref, R.; Buchwald, W. Sub-wavelength plasmonic modes in a conductor-gap-dielectric system with a nanoscale gap. *Opt. Express* **2010**, *18*, 348−363.

(27) Cui, S.; Zhang, X.; Liu, T.-l.; Lee, J.; Bracher, D.; Ohno, K.; Awschalom, D.; Hu, E. L. Hybrid Plasmonic Photonic Crystal Cavity for Enhancing Emission from near-Surface Nitrogen Vacancy Centers in Diamond. *ACS Photonics* **2015**, *2*, 465−469.

(28) Yang, Y.; Miller, O. D.; Christensen, T.; Joannopoulos, J. D.; Soljačić, M. Low-Loss Plasmonic Dielectric Nanoresonators. *Nano Lett.* **2017**, *17*, 3238−3245.

(29) Chen, W.; Thoreson, M. D.; Ishii, S.; Kildishev, A. V.; Shalaev, V. M. Ultra-thin ultra-smooth and low-loss silver films on a germanium wetting layer. *Opt. Express* **2010**, *18*, 5124−5134.

(30) Schell, A. W.; Kewes, G.; Schröder, T.; Wolters, J.; Aichele, T.; Benson, O. A scanning probe-based pick-and-place procedure for

DOI: 10.1021/acsphotonics.7b01194
ACS Photonics XXXX, XXX, XXX−XXX

assembly of integrated quantum optical hybrid devices. *Rev. Sci. Instrum.* **2011**, *82*, 073709.
(31) Jiang, Q.; Zhang, S.; Zhao, M. Size-dependent melting point of noble metals. *Mater. Chem. Phys.* **2003**, *82*, 225−227.
(32) Kurvits, J. A.; Jiang, M.; Zia, R. Comparative analysis of imaging configurations and objectives for Fourier microscopy. *J. Opt. Soc. Am. A* **2015**, *32*, 2082−2092.
(33) Neu, E.; Steinmetz, D.; Riedrich-Möller, J.; Gsell, S.; Fischer, M.; Schreck, M.; Becher, C. Single photon emission from silicon-vacancy colour centres in chemical vapour deposition nano-diamonds on iridium. *New J. Phys.* **2011**, *13*, 025012.
(34) Iwasaki, T.; et al. Germanium-Vacancy Single Color Centers in Diamond. *Sci. Rep.* **2015**, *5*, 12882.
(35) Manfrinato, V. R.; Wanger, D. D.; Strasfeld, D. B.; Han, H.-S.; Marsili, F.; Arrieta, J. P.; Mentzel, T. S.; Bawendi, M. G.; Berggren, K. K. Controlled placement of colloidal quantum dots in sub-15 nm clusters. *Nanotechnology* **2013**, *24*, 125302.
(36) Jiang, M.; Kurvits, J. A.; Lu, Y.; Nurmikko, A. V.; Zia, R. Reusable Inorganic Templates for Electrostatic Self-Assembly of Individual Quantum Dots, Nanodiamonds, and Lanthanide-Doped Nanoparticles. *Nano Lett.* **2015**, *15*, 5010−5016.
(37) Ramachandran, S.; Kristensen, P.; Yan, M. F. Generation and propagation of radially polarized beams in optical fibers. *Opt. Lett.* **2009**, *34*, 2525−2527.

DOI: 10.1021/acsphotonics.7b01194
ACS Photonics XXXX, XXX, XXX−XXX